Turbulent natural convection of a confined flow in a cubic enclosure: Effect of transient boundary conditions

A. Weppe, Florian Moreau, D. Saury

Cite as:

A. Weppe, F. Moreau, D. Saury, "Turbulent natural convection of a confined flow in a cubic enclosure: Effect of transient boundary conditions", International Communication of Heat and Mass Transfer, 142, 106637, 2023.
DOI: 10.1016/j.icheatmasstransfer.2023.106637

Turbulent natural convection of a confined flow in a cubic enclosure: effect of transient boundary conditions

A. Weppe, F. Moreau, D. Saury

Institut Pprime - UPR CNRS 3346, CNRS - ISAE-ENSMA - Université de Poitiers, BP 40109 - 86961 Chasseneuil Futuroscope, France

Abstract

This paper presents the experimental study of a turbulent natural convection air flow occurring inside an enclosure with an inner block partially heated. Unsteady boundary conditions are applied on the heated face of the block. This allows to achieve boundary conditions and flow regimes that can be relevant for industrial unsteady heating or cooling purposes. The maximum Rayleigh number reached is equal to 1.98×10^9 which corresponds, for instance, to the flow regime encountered in the underhood of cars. For Rayleigh numbers from 0.25×10^9 to 1.98×10^9, a dynamical analysis of the flow is conducted and similarity properties of the ascendant boundary layer are highlighted.

Email addresses: florian.moreau@ensma.fr (F. Moreau), didier.saury@ensma.fr (D. Saury)

Nomenclature

g	acceleration due to gravity, $\mathrm{m\,s^{-2}}$
Gr	Grashof number, $Gr = \frac{g\beta\Delta T H_{block}^3}{\nu^2}$
H_{block}	block height (reference length), m
L	enclosure length, m
P	power injected by the heating supply, W
$Ra_{H_{block}}$	Rayleigh number based on block height, $Ra_{H_{block}} = \frac{g\beta\Delta T H_{block}^3}{\nu\alpha}$
T	temperature, K
t	time, s
t_{obs}	observation time, s
t^*	dimensionless time, $t^* = t/\tau$
T_0	reference temperature, $T_0 = \frac{1}{2}(T_h + T_c)$, K
U, V, W	dimensionless velocities (scaled by $\alpha\sqrt{Ra_H}/\mathrm{H}$)
U_c	characteristic boundary layer velocity , $U_c(z^*) = \sqrt{g\beta\Delta T^+ z^*}$, $\mathrm{m\,s^{-1}}$
x, y, z	physical Cartesian coordinates, m
z^*	$z^* = z - 0.1$, 0.1 corresponds to the beginning of the elevation of the heated plate
X, Y, Z	dimensionless coordinates, $(X, Y, Z) = (x, y, z)/L$

Greek symbols

α	thermal diffusivity, $\mathrm{m^2\,s^{-1}}$
β	thermal expansion coefficient, $\mathrm{K^{-1}}$
δ	characteristic boundary layer thickness, m
ΔT	$\Delta T = T_h - T_c$, K
ΔT^+	$\Delta T^+ = T_h - T_0$, K
ε	emissivity
Φ	heat flux, W
λ	thermal conductivity, $\mathrm{W\,m^{-1}\,K^{-1}}$
ν	kinematic viscosity, $\mathrm{m^2\,s^{-1}}$
ρ	density, $\mathrm{kg\,m^{-3}}$
τ	characteristic heating time of the block, s

Subscripts and superscripts

amb	ambient
c	cold
h	hot
$\overline{X}$	time averaged value of X: $\overline{X} = \frac{1}{t_{\text{obs}}} \int_0^{t_{\text{obs}}} X(t)\, dt$

Abbreviations

DHC	Differentially Heated Cavity

1. Introduction

Natural convection in cavities has been extensively studied notably because of its presence in a large range of applications. However, turbulent buoyancy driven flows still remain challenging. In particular, it still lacks RANS models with low computational costs, which can properly predict interactions between buoyancy forces and turbulence. As a consequence, heat transfers are often badly quantified. The case of a buoyancy driven flow in an enclosure with an inner heated block is no exception. This configuration, often encountered in nuclear and automotive industries for instance, will be investigated in this study. It consists in a cubic enclosure with an inner and partially heated cubic block. Moreover, the block is heated to model transient heating/cooling processes. Some studies have been focusing on the role, on a buoyancy driven flow, of a block which is put inside an enclosure. For instance, House et al. [1] numerically studied, in two dimensions, the effects over heat transfers of the conductivity and length of a centered square block in a differentially heated square enclosure. When the block length is inferior to the stagnant core of the differentially heated cavity (DHC), it has been shown that heat transfers are reduced (resp. enhanced) for a low (resp. high) ratio of the block conductivity over the fluid's one. Ha and Jung [2] have studied, for a similar configuration but in three dimensions, the influence of an inner heated cubic block in a differentially heated cubic cavity. For a low ratio of the temperature generated by the block over the temperature difference generated by the DHC, the flow topology is similar to the one observed by House et al. [1], i.e. a rotating flow around the block. When this ratio is higher, recirculation zones are observed in the enclosure channels. Ha et al. [3] have also studied, in two dimensions, the transient behavior of an air flow inside an enclosure with a suddenly heated block. After the sudden heating, recirculation zones progressively appear inside the enclosure. Those numerical studies consider

laminar regimes ($Ra < 10^6$) into DHC with fully heated blocks. The influence of obstacles has also been studied in the Rayleigh-Bernard configuration, see for instance Chaabane et al. [4]. Turbulent regimes have been rather studied for differentially heated cavities and vertical channels without block. Those configurations are of interest, for the present study, since our configuration can be seen either as a succession of vertical/horizontal channels or cavities. Unstable flows in differentially heated cavities have been first investigated both numerically and experimentally ([5, 6, 7, 8]). The increasing amplitude of Tollmien-Schlichting waves observed in vertical boundary layers are notably responsible for the transition to a turbulent regime ([9]). Experimentally, Salat et al. [10] have studied turbulent flows ($Ra \geq 10^9$) in a cubic DHC. Separated boundary layer flows have been observed. The vertical ascending and descending boundary layers become turbulent from a certain elevation along the walls. Saury et al. [11] or Belleoud et al. [12, 13] later studied a higher Rayleigh number flow ($Ra = 1.2 \times 10^{11}$) in a vertical differentially heated cavity. Results have been compared to numerical simulations by Trias et al. [14] with good agreement. Recently, for an asymetrically heated channel, Thebault et al. [15, 16] have also observed low and medium frequency ranges associated with coherent structures which are responsible for the transition to a turbulent regime. Experimentally, transient heating/cooling in a differentially heated cavity or vertical channel has not been studied much, probably due to the complexity of its implementation. The block in our configuration is both partially and transiently heated. The present study with transiently heated boundary conditions follows a first one with steady boundary conditions and for a Rayleigh number, based on the inner block height, equal to $Ra_{H_{block}} = 1.37 \times 10^9$ ([17]).

2. Experimental set-up

The following section presents in details the enclosure, the transient boundary conditions and velocity measurement technique.

2.1. Enclosure description: Cavity and inner block

The studied experimental setup consist in a cubic vertical cavity of inner length $L = 1\,\mathrm{m}$ with an inner partially heated block. The cubic block, whose edge length is $H_{block} = 0.8\,\mathrm{m}$, is centered inside this DHC. Thus, it remains a distance $l = 0.1\,\mathrm{m}$ between the block walls and the enclosure walls. Figures 1,2

and 3 represent the experimental apparatus with a 2D and a 3D schemes and a photo. The physical coordinates are made dimensionless with L.

Two of the lateral enclosure walls are water heat exchangers ($\lambda = 174\,\mathrm{W\,m^{-1}\,K^{-1}}$, $\varepsilon = 0.10$). Two cooling bath circulators maintain them at a constant temperature, $T_c \approx T_{amb}$, in order to minimize heat transfer with the air surrounding the experimental set-up. T_c is regulated by the cooling systems that uses a Pt100 probe. Those systems allow to ensure uniform temperature on two opposite vertical surfaces. The other walls are considered adiabatic: the upper and lower enclosure walls are 10-cm-thick extruded polystyrene ($\lambda = 0.035\,\mathrm{W\,m^{-1}\,K^{-1}}$) and are covered with aluminum sheets in order to limit radiation effects ($\varepsilon = 0.08$). The rear and front walls are 6-mm-thick glass windows that allow flow visualization. The 6-cm-thick blocks of extruded polystyrene are put in front of them in order to ensure the adiabatic conditions.

Concerning the inner block: four polymer rods ($\lambda = 0.25\,\mathrm{W\,m^{-1}\,K^{-1}}$) maintain the block and limit conduction effects. They are put at every corner of the bottom part of the block in order to reduce possible perturbations in the vertical mid-depth plane where the measurements are made. The block is notably composed of two 4-cm-thick aluminum plates ($\lambda = 174\,\mathrm{W\,m^{-1}\,K^{-1}}$) which form the lateral block sides facing the two cavity isothermal plates (maintained at T_c). One of those aluminum block plates is heated at a temperature T_h by a heating wire. T_h is measured inside the aluminium plate using a K-type thermocouple. T_h varies in time to obtain an unsteady boundary condition (see section 2.2). A succession of Rockwool panels, Ertalon and POM-C plates are put between the two aluminium plates. Those elements provide both the block's mechanical strength and thermal insulation. The temperature, inside the block, decreases between the two aluminium plates. The characteristic heating time, τ, of the block is equal to $\tau = 242\,\mathrm{min}$. 4-mm-thick POM-C plates cover the rear, front, lower and upper block walls in order to preserve a good surface condition. Low-emissivity aluminium sheets cover those surfaces ($\varepsilon = 0.08$).

2.2. Heated plate temperature variation and measurements campaign

The temperature difference, $\Delta T = T_h - T_c$, between the block heated plate, at T_h, facing one of the enclosure plate at T_c, creates the fluid motion in the enclosed space. The Rayleigh number used in this study is based on the block height, H_{block}: $Ra_{H_{block}} = \frac{g\beta\Delta T H_{block}^3}{\alpha\nu}$, where g is the acceleration due to gravity, β is the thermal expansion coefficient, α is its thermal diffusivity, ν is

its kinematic viscosity. The heating wire is powered by a controllable power supply PS 8000 2U Elektro-Automatik®. It is controlled by a Labview® program which allows to choose the injected power. The experimental protocol for the present study consists in injecting and maintaining a weak initial power (P=12W) before starting the experiment ($t = 0$) in order to get a reproductible air flow inside the enclosure and stabilized boundary conditions. At $t = 0$, the power is then suddenly increased ($P(t \geq 0) = 493\,\mathrm{W}$). This results in an increase of the temperature difference ΔT with time (see Fig. 4). Multiple sets of measurements are carried out for different times $t^* = t/\tau$ during the experiment (thus corresponding to different $\Delta T = T_h - T_c$). Between the beginning and the end of an experiment, ΔT varies from 4.6 to 53.4 °C and thus t^* from 0 to 0.56 (see Table 1). This leads to a variation of Ra from 0.25×10^9 to 1.98×10^9. A set of measurements corresponds to 5000 images obtained at 25 Hz ($t_{\mathrm{obs}} = 200\,\mathrm{s}$). During a set of measurements, the heated plate temperature, T_h, can increase up to 1.5 °C. In the following sections, the heated plate temperature is thus temporally averaged on an acquisition time. The measurement campaigns are carried out in the two vertical channels of the enclosure named the heated vertical channel and the unheated vertical channel (see Fig. 1 and 2).

2.3. Velocity measurements

Velocities are determined by using Particle Image Velocimetry (PIV) measurements. The laser is a pulsed laser Nd: YAG ($2\times50\,\mathrm{mJ@100\,Hz}$). It generates a light sheet in the mid-depth plane of the enclosure. The vertical mid-depth plane is located at $X = 0.5$ (see Fig. 2) A smoke generator produces particles which are injected into the enclosed space through a small hole located into the upper enclosure wall. This hole is then closed. Those seed particles are paraffine oil particles. They are appropriate tracers since $\frac{V_s}{V_{max}} \simeq 1.5 \times 10^{-3}$ where V_s is the settling velocity and V_{max} is the maximum velocity in the flow. A camera MX $5120 \times 5120\,\mathrm{pixels}^2$ captures the reflected light of the particles impacted by the laser. The field size is chosen to be $490 \times 100\,\mathrm{mm}^2$ in order to both get a good enough resolution for the PIV algorithm and capture the largest possible height of the two vertical channels where the measurements are carried out. The velocities are made dimensionless with $V_{ref} = \frac{\alpha}{H_{block}}\sqrt{Ra_{H_{block}}}$ determined at $\Delta T(t < 0) = 4.6\,°\mathrm{C}$.

3. Results

In this section, the dynamical behavior of the flow is described in both the heated and unheated vertical channels and similarity properties of the ascendant boundary layer are highlighted.

3.1. Dynamical behavior in the heated vertical channel

The norm of the mean velocity fields at different dimensionless times t^* and temperature differences ΔT in the heated vertical channel are plotted in Figure 5. For the initial and stabilized regime ($\Delta T(t < 0) = 4.6\,^{\circ}\mathrm{C}$), boundary layer flows can be found near the hot and cold plates with higher velocities in the ascending boundary layer. When the hot boundary layer flow reaches the end of the hot plate, it either goes to the upper horizontal channel or moves toward the cold plate. There, it begins to go downward. When it reaches the enclosure bottom, it then fuels the beginning of the ascending boundary layer. Moreover, in the lower part of the heated vertical channel, the center of a large recirculation zone is observed. However, in the center of the channel, velocities are near 0. With ΔT (or t^*) increasing, a recirculation area, at $Z = 0.95$, progressively appears in the upper part of the channel and is clearly visible for $\Delta T = 13.2\,^{\circ}\mathrm{C}$. This top-recirculation zone grows with ΔT and reaches $Z \approx 0.60$ for $\Delta T = 53.4\,^{\circ}\mathrm{C}$. It can also be noted the formation of a singular zone which first appears from $\Delta T = 21.2\,^{\circ}\mathrm{C}$, at $Y \approx 0.05$ and $Z \approx 0.70$. This singular zone grows with ΔT and slightly moves. For $\Delta T \geq 30.7\,^{\circ}\mathrm{C}$, this zone seems to affect the shape of the recirculation zone. Velocities in this singular zone are nonetheless near 0. In the lower part of the heated vertical channel, no major change in the flow topology is observed with ΔT increasing. The descending flow along the cold plate fuels the forming ascendant boundary layer regardless of ΔT.

Figure 6 shows horizontal profiles of the mean vertical velocity at $Z = 0.80$ and vertical profiles of the mean horizontal velocity at $Y = 0.05$ for different ΔT. Vertical bars represent the uncertainty on the maximum vertical velocity. The ascendant boundary layer along the hot wall at T_h is developing as ΔT increases. With ΔT growing, buoyancy forces keep increasing. From $\Delta T = 9.2\,^{\circ}\mathrm{C}$ to $\Delta T = 53.4\,^{\circ}\mathrm{C}$, the maximum of the mean vertical velocity is multiplied by 2.14 (respectively $\overline{W} = 0.59$ and $\overline{W} = 1.27$). A diminution of the boundary layer thickness is also spotted with the increase of ΔT. This phenomenon has already been observed for boundary layers developing along vertical plates by Le Quéré [18]. It is explained by a balance between viscous

and Archimedes forces in the viscous sublayer. Along the cold plate at T_c, a descending flow is observed where the minimum of the vertical velocity is multiplied by 2.7 between $\Delta T = 9.2\,^{\circ}\mathrm{C}$ and $\Delta T = 53.4\,^{\circ}\mathrm{C}$ (respectively $\overline{W} = -0.13$ and $\overline{W} = -0.36$).
The horizontal mean velocity component $\overline{V}$, plotted for $Y = 0.05$, shows a developing wall jet along the top wall. When looking at $Z \in [0.7; 0.9]$, the recirculation zone can be observed for $\Delta T > 9.2\,^{\circ}\mathrm{C}$. It is worth mentioning that for $\Delta T = 4.6\,^{\circ}\mathrm{C}$ and $\Delta T = 9.2\,^{\circ}\mathrm{C}$, the horizontal velocity is still negative $\overline{V} \leq 0$ whereas when ΔT reaches $\Delta T = 13.2\,^{\circ}\mathrm{C}$, the mean horizontal velocity component ($\overline{V}$) becomes positive for $Z \in [0.84; 0.93]$. This corresponds to the onset of the recirculation area. This zone of positive horizontal velocity grows with ΔT as already observed in Figure 5. For $Z < 0.70$, the horizontal velocity is near 0.

Figure 7 shows horizontal profiles of the mean vertical velocity at $Z = 0.20; 0.40; 0.60; 0.80$ and for the different ΔT studied. In particular, for a given ΔT, the vertical velocity in the ascending boundary layer is increasing with Z. This is a classic behavior for a boundary layer developing along a vertical plate. On the contrary, the absolute value of the minimum vertical velocity along the descending boundary layer reduces with Z decreasing. The same behavior has already been observed for the stationary regime (see Weppe et al. [17]). This behavior is probably due to the fact that the temperature difference between the cold plate and the vertical channel core is smaller with Z decreasing. The buoyancy forces are thus less important along the cold plate and are not able to compensate the viscous diffusion along this plate. It results in a decrease of the mean vertical velocity.

3.2. Scaling

Similarity properties of the ascendant boundary layer are studied in this section. The scaling considered is similar to the one used to study the similarity properties of a spatially developing laminar boundary layer along a vertical plate ([19, 20]). The mean vertical velocity and the distance from the plate are thus respectively made dimensionless with U_c a characteristic boundary layer velocity and with δ a characteristic boundary layer thickness, defined as:

$$U_c(z^*) = \sqrt{g\beta\Delta T^+ z^*} \quad ; \quad \delta(z^*) = \frac{z^*}{Gr(z^*)^{\frac{1}{4}}} \tag{1}$$

with $\Delta T^+ = T_h - T_0$, $T_0 = \frac{T_h+T_c}{2}$, and $z^* = z - 0.1$ (the value 0.1 corresponds to the beginning of the elevation of the heated plate). Gr is the local Grashof number.

This scaling can also be used for turbulent boundary layers ([21, 22]). Figure 8 shows the evolution of the mean vertical dimensionless velocity ($\overline{w}/U_c$) versus the dimensionless distance from the heated plate ($(0.1 - y)/\delta$), for several temperature differences and elevations. Moreover, on each graph is inserted the mean vertical velocity made dimensionless with V_{ref} ($\overline{W}$) versus Y and for the same ΔT. The scaling of the vertical velocity with U_c makes the curves approximately collapse into a single one. For instance, the maximum deviation between the maximum of the dimensionless vertical velocity ($\overline{w}_{max}/U_c$) at $Z = 0.80$ is equal to $\epsilon_{max} = 10.1\%$ while it is equal to $\epsilon_{max} = 114\%$ regarding the evolution of $\overline{W}_{max}$. The vertical profile thus shows similarity properties. With the scaling by δ, the evolution of the boundary layer thickness is also approaching a unique evolution. The same observations can be made for $Z = 0.20; 0.40; 0.60$. It confirms the possible use of this boundary layer scaling along a vertical plate to study similarity properties of the ascending boundary layer in the heated channel. Nevertheless, a significant deviation between the boundary layer thicknesses is noticeable for $Z = 0.20$. This deviation probably comes from a difference in the fuelling of the ascending boundary layer of this differentially unsteadily heated channel compared to a more conventional developing boundary layer along a vertical hot plate.

3.3. Dynamical behavior in the unheated vertical channel

The norm of the mean dimensionless velocity fields at different ΔT in the unheated vertical channel are plotted in Figure 9. For the initial and stabilized regime ($\Delta T = 4.6\,^{\circ}\mathrm{C}$), a descending flow that comes from the top horizontal channel is observed along the cold plate at T_c and $Y \approx 0.99$. Along the unheated block plate ($Y = 0.9$), the flow behavior is more complex. It consists in a descending flow along the unheated plate between $Z = 0.90$ and $Z \approx 0.65$ and an ascending flow between $Z = 0.10$ and $Z \approx 0.65$. When ΔT increases, the position of the separation zone between the ascending and descending flow along the block keeps lowering. In fact, the flow coming from the upper horizontal channel is certainly hotter when ΔT is increasing (as observed in the heated channel). Thus, the descending flow along the block travels a greater distance before reaching the block's temperature. From there, the

buoyancy forces vanish. The descending flow thus slows down before meeting the ascending flow which also experiences cooling along the block. The two flows then direct to the cold plate. Moreover, it can also be seen the lowering of a recirculation zone in the lower part of the vertical channel.

Figure 10 shows horizontal profiles of the mean vertical dimensionless velocity at $Z = 0.80, 0.60, 0.40$ and 0.20. At $Z = 0.80$, separated descending flows can be observed. When increasing the temperature difference ΔT, the descending flows along the cold plate and the block are getting thinner. Moreover, the absolute value of the velocity maximum is increased. At $Z = 0.60$ and the stabilized regime ($\Delta T = 4.6\,^{\circ}\mathrm{C}$), the vertical component of the velocity along the block is slightly positive. It shows that for this particular elevation, the flow is indeed in the separation zone already observed in Figure 9. For lower Z, the same phenomenon is observed. Furthermore, at $Z = 0.40$ and $Z = 0.20$, the ascending flow along the block and the descending flow along the cold plate are not separated anymore. It highlights the recirculation zone effect.

4. Conclusions

In this paper, a transient turbulent natural convection flow inside a cubic enclosure with a partially heated inner block is investigated. The influence of the transient heating of a face of the block is highlighted. During this transient heating, the temperature difference between the heated face of the block and the opposite cold plate of the cavity varies from $\Delta T = 4.6$ to 53.4 °C. This leads to a variation of the Rayleigh number based on the height of the block ranging from $Ra = 0.25 \times 10^9$ to 1.98×10^9. This corresponds to the turbulent regimes encountered in industrial context like the underhood of cars for instance. PIV measurements are conducted in the mid-depth vertical plane of the vertical heated and unheated channels. The following conclusions can be drawn:

— During the transient heating, as ΔT increases, boundary layer flows are spatially and temporally developing along the vertical hot and cold plates. A recirculation area gradually emerges in the top part of the heated channel.

— The dynamics of the ascendant boundary layer in the heated vertical channel layer have similarity properties that are well described by a scaling law. This scaling law, previously used in the literature for laminar and turbulent boundary layer developing along a vertical plate, is extended here to transient boundary conditions and in a more complex geometry.

— The complex evolution of the flow in the vertical unheated channel is also described. In particular, a descending flow coming from the top horizontal channel and an ascending flow coming from the bottom of the unheated channel encounter along the block. As ΔT increases, the separation zone between those flows is lowered. This is due to the intensification of the hot flow coming from the heated channel through the top horizontal channel.

5. Acknowledgments

The authors would thank the ANR MONCACO_2025 grant (ANR-17-CE06-0005) for supporting this work as well as the "transport" CPER/FEDER Program. The authors would also like to thank H. Arlaud, J.-C. Fraudeau, N. Papin and C. Fuentes.

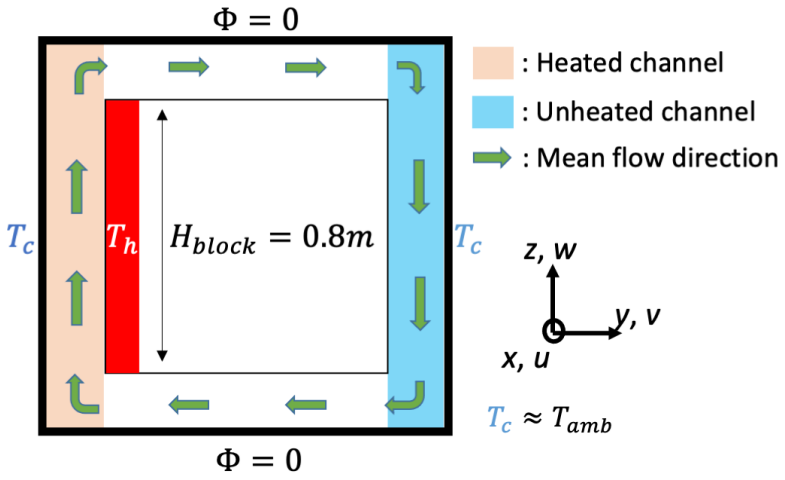

FIGURE 1 – 2D scheme of the experimental set-up.

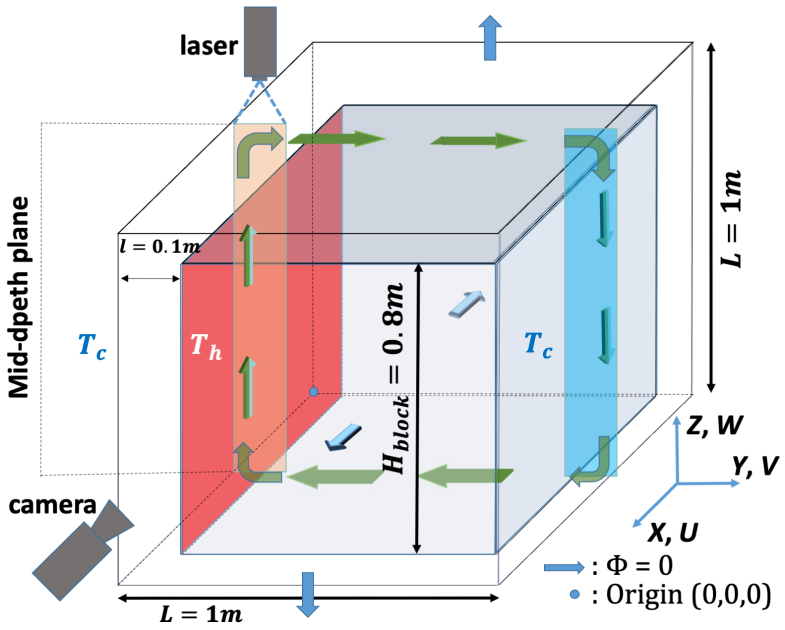

FIGURE 2 – 3D scheme of the experimental set-up.

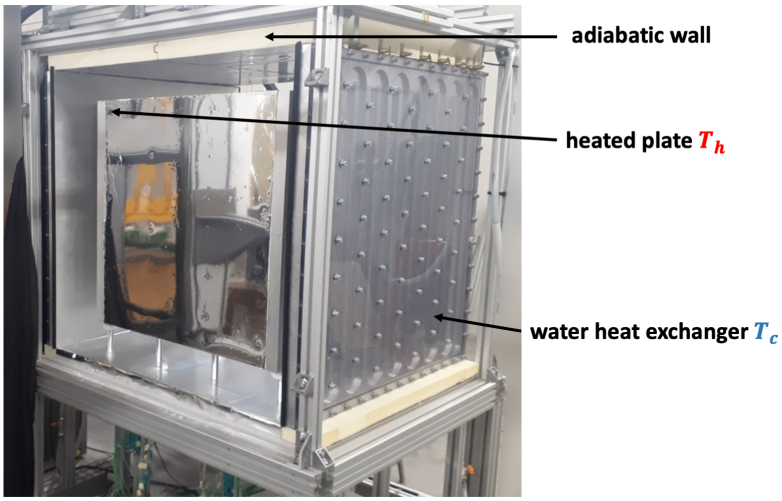

FIGURE 3 – Photo of the experimental set-up

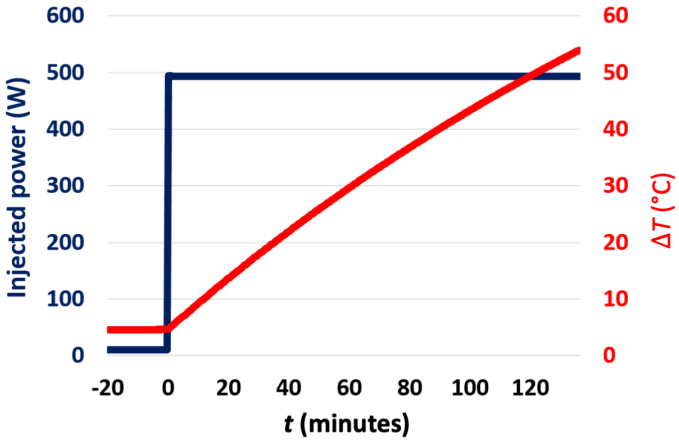

FIGURE 4 – Injected power and temperature difference ΔT evolution

ΔT	$t^* = t/\tau$	$Ra_{H_{block}}(\times 10^9)$
4.6°C	0	0.25
9.2°C	0.04	0.47
13.2°C	0.08	0.66
21.2°C	0.16	1.00
25.1°C	0.20	1.15
30.7°C	0.26	1.34
37.2°C	0.34	1.55
53.4°C	0.56	1.98

TABLE 1 – Temperature differences studied with corresponding dimensionless times and Rayleigh numbers

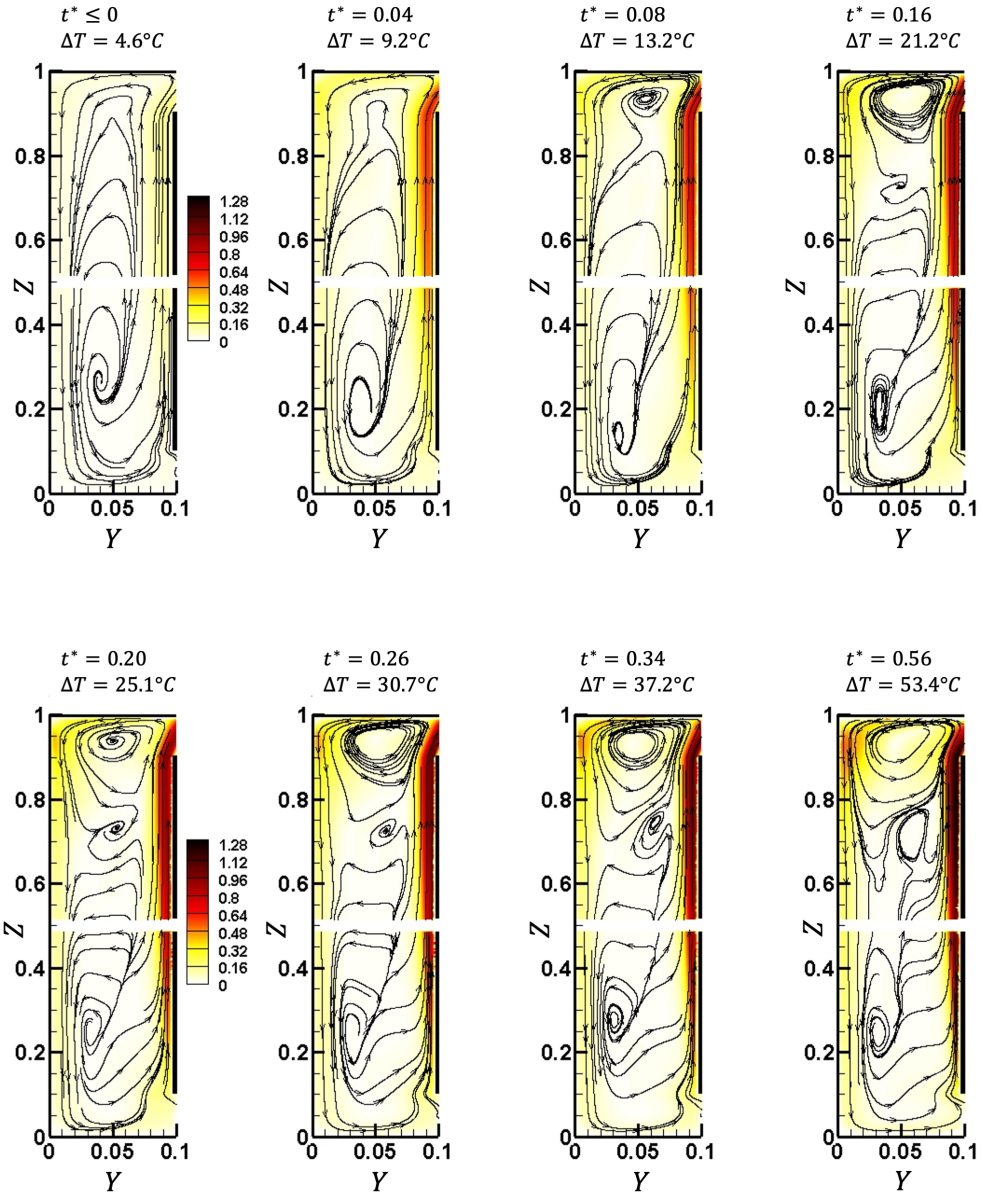

FIGURE 5 – Norm of the mean velocity fields and streamtraces from $\Delta T = 4.6°\text{C}$ to $\Delta T = 53.4°\text{C}$ (mid-depth plane of the heated vertical channel)

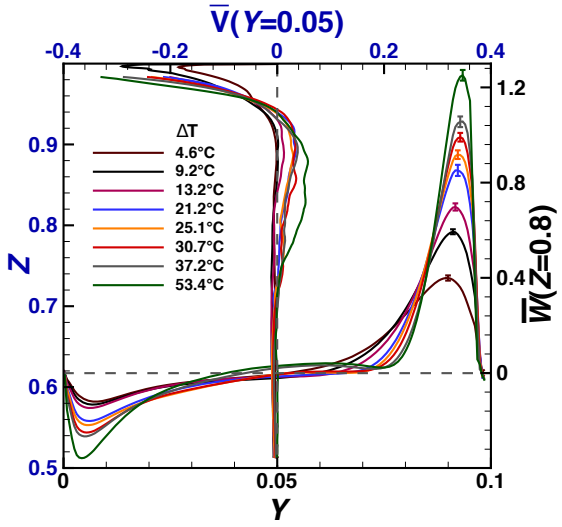

FIGURE 6 – Horizontal and vertical mean velocity profiles (at $Y = 0.05$ and $Z = 0.8$) from $\Delta T = 4.6$°C to $\Delta T = 53.4$°C (mid-depth plane of the heated vertical channel). Vertical bars represent the uncertainty on the maximum vertical velocity.

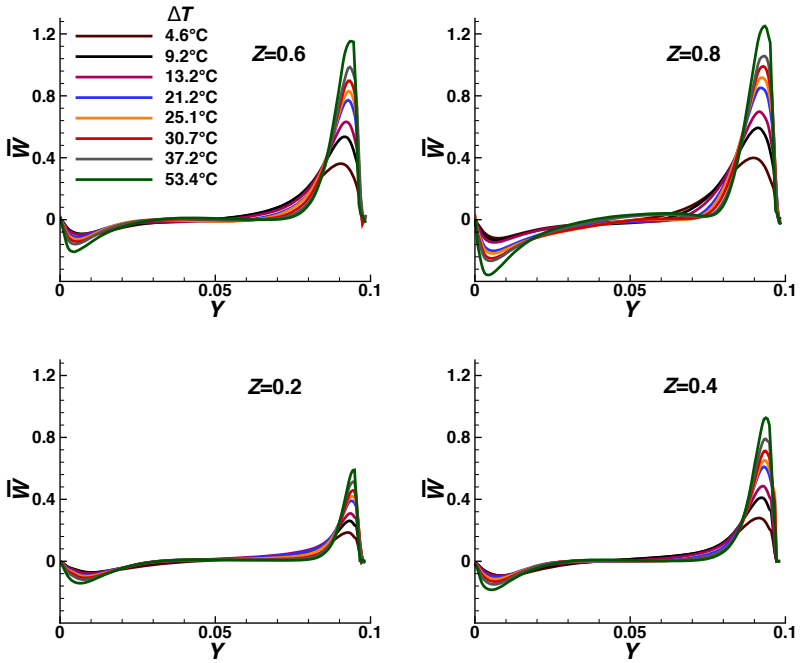

FIGURE 7 – Vertical mean velocity profiles (for $Z = 0.2$, $Z = 0.4$, $Z = 0.6$, $Z = 0.8$) from $\Delta T = 4.6$°C to $\Delta T = 53.4$°C (mid-depth plane of the heated vertical channel)

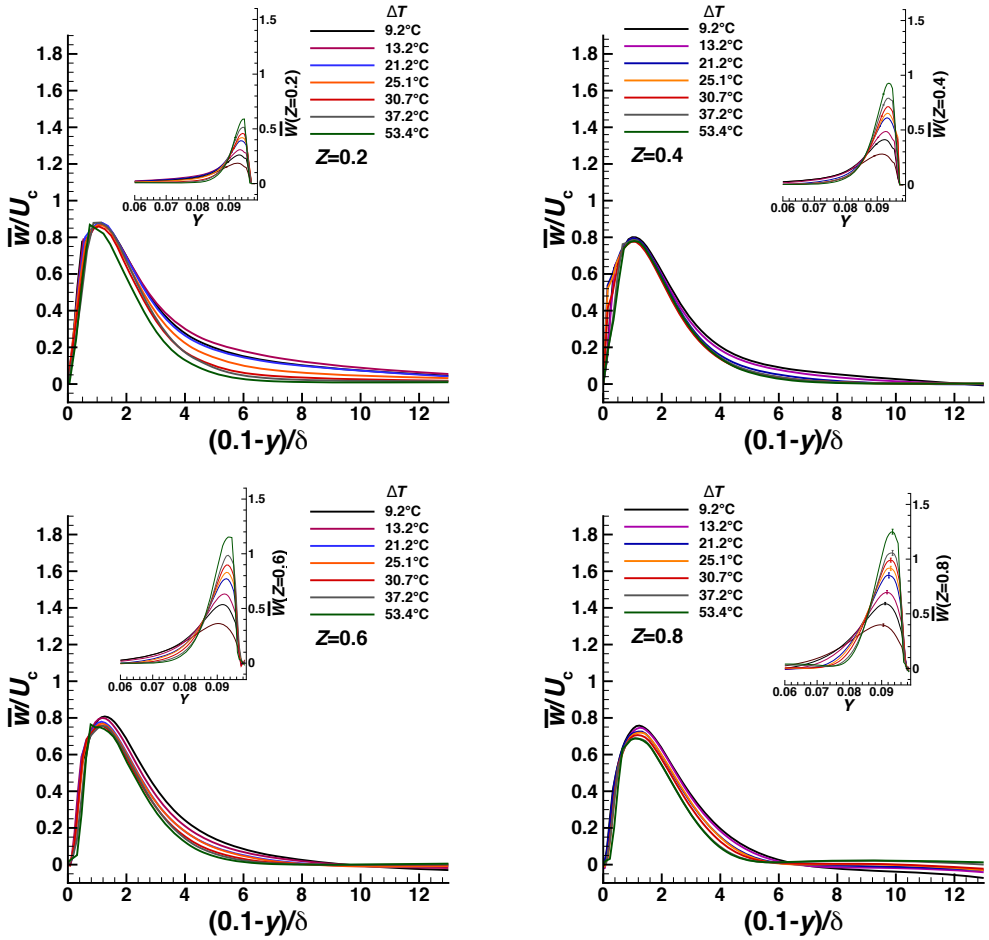

FIGURE 8 – Horizontal profiles of the dimensionless vertical mean velocity ($\overline{w}/U_c$) for $Z = 0.2; 0.4; 0.6; 0.8$ and for ΔT from 4.6°C to 53.4°C vs $(0.1 - y)/\delta$ (mid-depth plane). Inset of the dimensionless vertical mean velocity ($\overline{W}$ vs. Y)

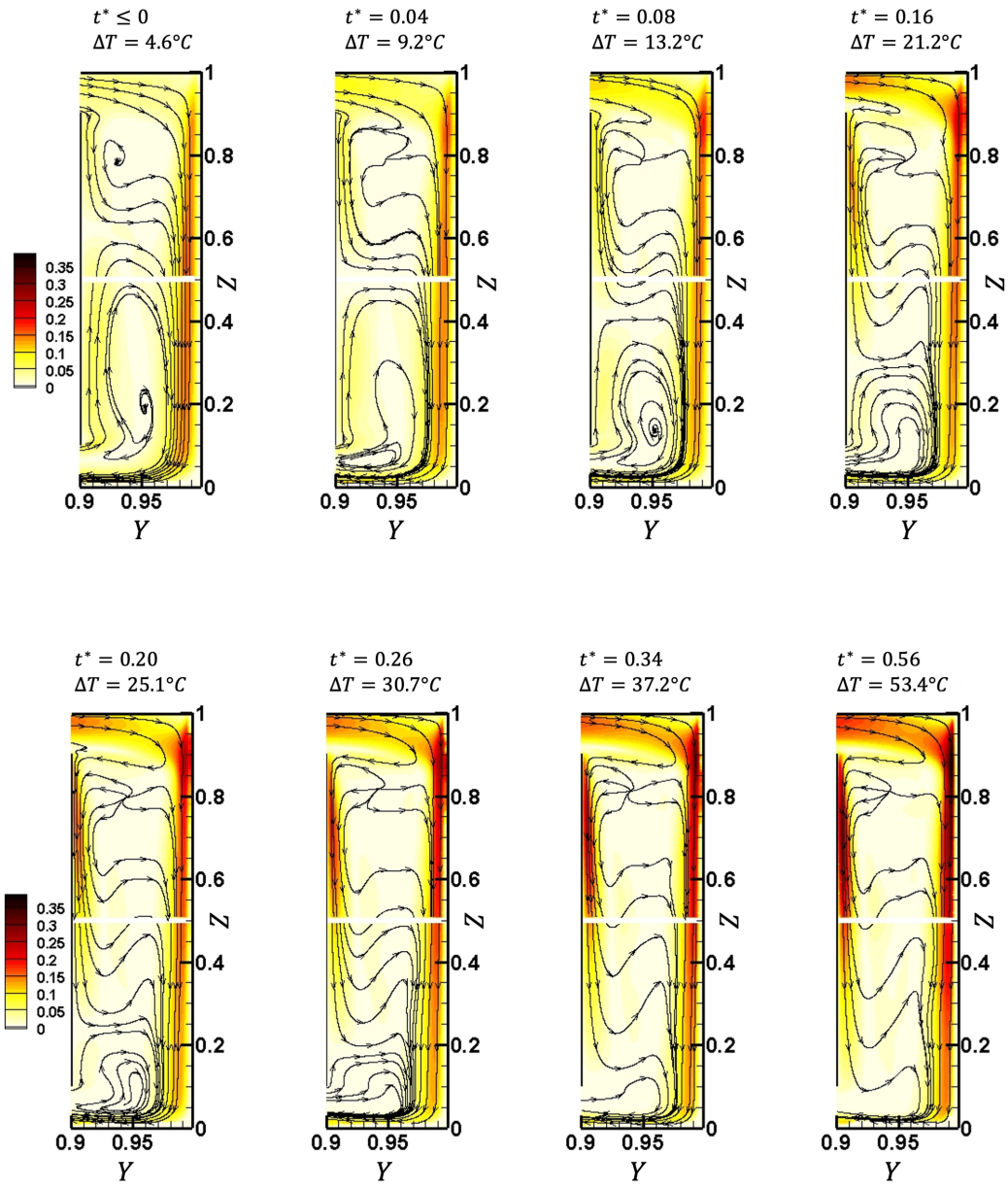

FIGURE 9 – Norm of the mean velocity fields and streamtraces from $\Delta T_m = 4.6°\text{C}$ to $\Delta T_m = 53.4°\text{C}$ (mid-depth plane of the unheated vertical channel)

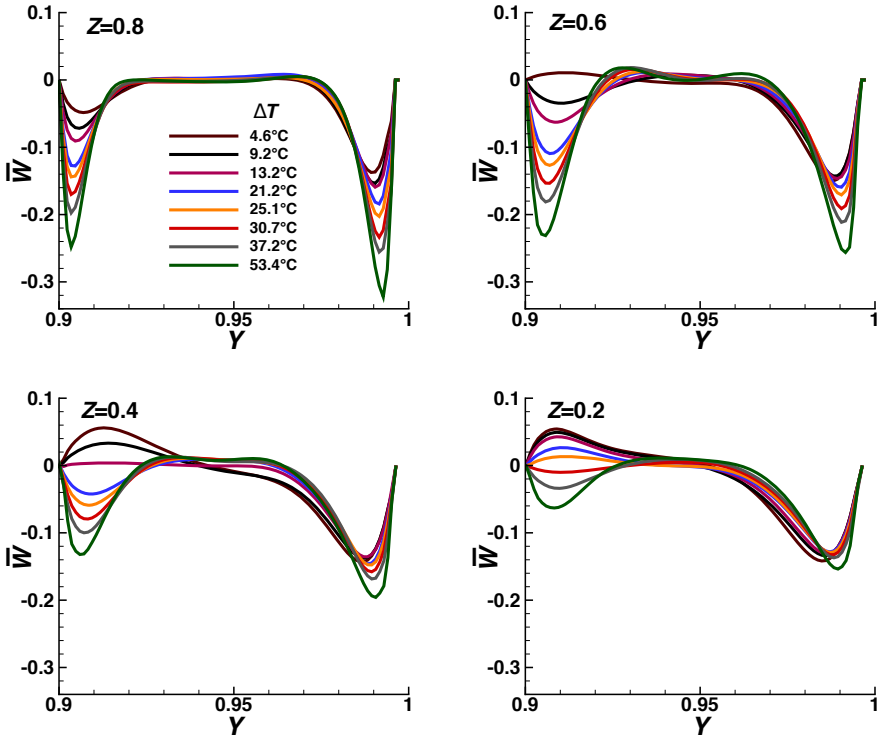

FIGURE 10 – Vertical mean velocity profiles (for $Z = 0.8$, $Z = 0.6$, $Z = 0.4$, $Z = 0.2$) from $\Delta T = 4.6°\text{C}$ to $\Delta T = 53.4°\text{C}$ (mid-depth plane of the unheated vertical channel)

Références

[1] J. M. House, C. Beckermann, and T. F. Smith, "Effect of a Centered Conducting Body on Natural Convection Heat Transfer in an Enclosure," *Numerical Heat Transfer, Part A : Applications*, vol. 18, no. 2, pp. 213–225, 1990.

[2] M. Y. Ha and M. J. Jung, "A numerical study on three-dimensional conjugate heat transfer of natural convection and conduction in a differentially heated cubic enclosure with a heat-generating cubic conducting body," *International Journal of Heat and Mass Transfer*, vol. 43, no. 23, pp. 4229–4248, 2000.

[3] M. Y. Ha, M. J. Jung, and Y. S. Kim, "Numerical Study on Transient Heat Transfer and Fluid Flow of Natural Convection in an Enclosure with a Heat-Generating Conducting Body," *Numerical Heat Transfer, Part A : Applications*, vol. 35, no. 4, pp. 415–433, 1999.

[4] R. Chaabane, L. Kolsi, A. Jemni, N. K. Alshammari, and A. D'Orazio, "Numerical study of the rayleigh–bénard convection in two-dimensional cavities heated by elliptical heat sources using the lattice boltzmann method," *Physics of Fluids*, vol. 33, no. 12, p. 123605, 2021.

[5] S. Paolucci and D. R. Chenoweth, "Transition to chaos in a differentially heated vertical cavity," *Journal of Fluid Mechanics*, vol. 201, pp. 379–410, 1989.

[6] S. Paolucci, "Direct numerical simulation of two-dimensional turbulent natural convection in an enclosed cavity," *Journal of Fluid Mechanics*, vol. 215, pp. 229–262, 1990.

[7] P. Le Quéré and M. Behnia, "From onset of unsteadiness to chaos in a differentially heated square cavity," *Journal of Fluid Mechanics*, vol. 359, pp. 81–107, 1998.

[8] S. Mergui and F. Penot, "Convection naturelle en cavité carrée différentiellement chauffée : investigation expérimentale à $Ra = 1{,}69 \times 10^9$," *International Journal of Heat and Mass Transfer*, vol. 39, no. 3, pp. 563–574, 1996.

[9] S. Xin and P. Le Quéré, "Direct numerical simulations of two-dimensional chaotic natural convection in a differentially heated cavity of aspect ratio 4," *Journal of Fluid Mechanics*, vol. 304, pp. 87–118, 1995.

[10] J. Salat, S. Xin, P. Joubert, A. Sergent, F. Penot, and P. Le Quéré, "Experimental and numerical investigation of turbulent natural convection in a large air-filled cavity," *International Journal of Heat and Fluid Flow*, vol. 25, no. 5, pp. 824–832, 2004.

[11] D. Saury, N. Rouger, F. Djanna, and F. Penot, "Natural convection in an air-filled cavity : Experimental results at large Rayleigh numbers," *International Communications in Heat and Mass Transfer*, vol. 38, no. 6, pp. 679–687, 2011.

[12] P. Belleoud, D. Saury, P. Joubert, D. Lemonnier, and F. Djanna, "Experimental investigations in an air-filled differentially-heated cavity at large Rayleigh Numbers," *Journal of Physics : Conference Series*, vol. 395, p. 012119, 2012.

[13] P. Belleoud, D. Saury, and D. Lemonnier, "Coupled velocity and temperature measurements in an air-filled differentially heated cavity at ra=1.2e11," *International Journal of Thermal Sciences*, vol. 123, pp. 151–161, 2018.

[14] F. X. Trias, M. Soria, A. Oliva, and C. D. Pérez-Segarra, "Direct numerical simulations of two- and three-dimensional turbulent natural convection flows in a differentially heated cavity of aspect ratio 4," *Journal of Fluid Mechanics*, vol. 586, pp. 259–293, 2007.

[15] M. Thebault, S. Giroux-Julien, V. Timchenko, C. Ménézo, and J. Reizes, "Transitional natural convection flow in a vertical channel : Impact of the external thermal stratification," *International Journal of Heat and Mass Transfer*, vol. 151, p. 119476, 2020.

[16] M. Thebault, S. Giroux-Julien, V. Timchenko, J. Reizes, and C. Ménézo, "Numerical study of the coherent structures in a transitional vertical channel natural convection flow," *Physics of Fluids*, vol. 33, no. 3, p. 034106, 2021.

[17] A. Weppe, F. Moreau, and D. Saury, "Experimental investigation of a turbulent natural convection flow in a cubic cavity with an inner obstacle partially heated," *International Journal of Heat and Mass Transfer*, vol. 194, p. 123052, 2022.

[18] P. Le Quéré, "Etude de la transition à l'instationnarité des écoulements de convection naturelle en cavité verticale différentiellement chauffée par méthodes spectrales chebyshev," PhD thesis, Poitiers, 1987.

[19] J. D. Hellums and S. W. Churchill, "Transient and steady state, free and natural convection, numerical solutions : Part i. the isothermal, vertical plate," *AIChE Journal*, vol. 8, no. 5, pp. 690–692, 1962.

[20] M. Z. Abedin, T. Tsuji, and Y. Hattori, "Direct numerical simulation for a time-developing natural-convection boundary layer along a vertical flat plate," *International Journal of Heat and Mass Transfer*, vol. 52, no. 19, pp. 4525–4534, 2009.

[21] T. Tsuji and Y. Nagano, "Velocity and temperature measurements in a natural convection boundary layer along a vertical flat plate," *Experimental Thermal and Fluid Science*, no. 2, pp. 208–215, 1989.

[22] Y. Hattori, T. Tsuji, Y. Nagano, and N. Tanaka, "Turbulence characteristics of natural-convection boundary layer in air along a vertical plate heated at high temperatures," *International Journal of Heat and Fluid Flow*, vol. 27, no. 3, pp. 445–455, 2006.